

high transfer efficiency [7–12]. For traditional second-order PT-symmetric systems, the near-field coupling induces frequency splitting in the strong coupling region, which requires active frequency tracking [13, 14] or utilizing non-linearities [15, 16] to maintain optimal power transfer efficiency. As the transfer distance increases, the system has a fixed working frequency in the weak coupling region, but the efficiency rapidly diminishes due to the complex eigenvalues. In 2017, Assaworrorarit *et al.* [17] experimentally revealed robust WPT based on a non-linear PT-symmetric circuit to track the real-time working frequency. However, efficient energy transfer in the weak coupling region is still a challenge [18]. Moreover, WPT systems with non-linear circuit components necessitate high-power technical input signals, making them challenging to implement in many high-power application scenarios. Recently, high-order systems have been extensively studied to solve the above problems [19, 20]. For instance, the system with the third-order PT-symmetry always has a purely real eigenvalue, so that can maintain high transfer efficiency even in weak coupling region [21, 22]. Nevertheless, PT-symmetric WPT systems remain limited to demanding operational requirements, due to the reliance on an inherently balanced configuration, which means the balance between gain and loss. The third-order systems even simultaneously require gain-loss balance and coupling symmetry, which severely restricts their applications. Additionally, traditional second-order systems exhibit serious field leakage from the transmitter coil in the strong coupling region, thus leading to poor electromagnetic compatibility. As a technical challenge, the realization of compact devices with great design freedom is still a significant challenge in practical engineering [23]. Therefore, linear non-Hermitian systems that eliminate PT-symmetry requirements, field leakage and integration complexities are exceptionally valuable.

As a localized, non-radiative eigenstate that coexists with a continuous spectrum of propagating waves, bound state in the continuum (BIC) has attracted great attention in recent years [24–26]. Unlike conventional bound states confined by potential barriers or bandgaps, BICs theoretically exhibit infinite quality- (Q -)factors by decoupling from radiative channels through symmetry protection, destructive interference, or topological constraints [27, 28]. BIC modes enhance electromagnetic wave confinement, minimizing leakage into free space and thus facilitating efficient energy transfer. Owing to its superior performance, BIC mode has rapidly accelerated the development of non-radiative WPT systems [29].

In this work, we exploit BIC in a high-order non-Hermitian system constructed by a composite transmitter (CT) and a single receiver (SR) to realize efficient WPT. The system always has a fixed working frequency regardless of transfer distance variations, which is significantly superior to the distance-dependent second-order

system constructed by a conventional single transmitter (ST) and SR. It should be noted that the working frequency known as BIC is a purely real eigenmode guaranteed by an optimal gain or loss, no matter whether the system satisfies PT-symmetry. The load can be adaptively tuned to accommodate varying distances between the CT and SR to realize the BIC mode for high-efficiency WPT. The CT structure can not only realize highly integrated system, but also enhance the electromagnetic compatibility of the transmitter. Our research conclusively demonstrates the applications of BIC in WPT system and provides a compact linear platform for highly efficient WPT.

2 Results

The traditional second-order WPT scheme with two coils is shown in Fig. 1(a). The power transfer from the ST to the SR, both resonant frequencies are ω_0 . The near-field coupling strength κ_0 between ST and SR depends on the transfer distance. The corresponding effective circuit model is shown in Fig. 1(b), where the ST (left circuit) and SR (right circuit) are coupled with the help of mutual inductance M between the distributed inductance L_1 and L_2 . Two-level scheme of the system with ST structure is shown in Fig. 1(c). Two resonant modes with the same resonant frequency ω_0 couple with each other. The near-field coupling κ_0 results in the splitting of frequency in the strong coupling region, which is called level-repulsion. The variable working frequency is impractical for applications. Here, we propose a flexible platform composed of the circuit-based third-order system to overcome frequency deviation. The circuit-based system constructed by CT and SR is shown in Fig. 1(d). The coupling strength κ_0 between CT and SR depends on the transfer distance, while the inner coupling in CT depends on the circuit. Figure 1(e) shows the corresponding effective circuit model of the synthetic third-order WPT system, where the coupling between L_1 and L_2 in CT is realized by C_0 . The CT (left circuit) and SR (right circuit) are coupled with the help of mutual inductance M between the distributed inductance L_2 and L_3 . Three-level scheme of the system with CT structure is shown in Fig. 1(f). The CT provides two detuning modes ($\omega_0 + \Delta$, $\omega_0 - \Delta$), which couple with the third mode provided by SR. The coupling strength of the detuned modes and the resonance mode is κ_{\pm} . γ and Δ denote the dissipative coupling and detuning factor of the resonance frequency in the CT structure, respectively. It can be seen that the position of the resonant mode ω_0 is always maintained, which is called level pinning (details about the level pinning of the third-order system are provided in the Supplementary Note 1) [30]. The phenomenon is enabled by the competition between the level attraction of the dissipative coupling

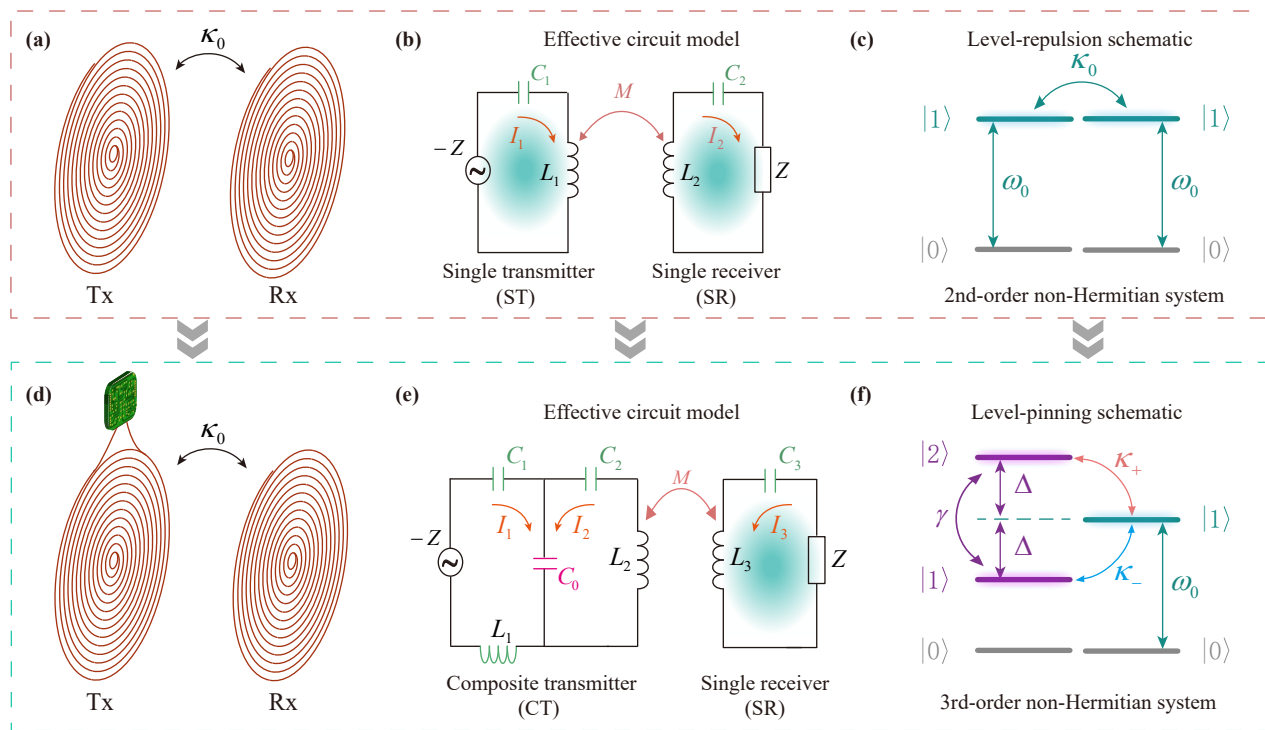


Fig. 1 Schematic diagram of the effective second-order ST-SR system and third-order CT-SR system. (a) The traditional second-order WPT scheme with ST and SR. (b) The effective circuit diagram of (a). The ST (left circuit) and SR (right circuit) are coupled with the help of mutual inductance M . (c) Energy Level diagram of (a). Coupling strength between the two resonant modes with the same frequency ω_0 is κ_0 . (d) Scheme of the novel third-order WPT scheme with CT and SR, which is composed of a distributed inductance and lumped elements. (e) The effective circuit diagram of (d). The inner coupling between L_1 and L_2 in CT is realized by C_0 . The coupling between distributed inductance L_2 and L_3 is realized by mutual inductance M . (f) Energy Level diagram of (d). The CT provides two modes $\omega_0 + \Delta$ and $\omega_0 - \Delta$, where coupling between the two detuning modes is imaginary coupling represented by $i\gamma$. The coupling between the two detuning modes and the third mode provided by SR is real coupling, which are represented by κ_{\pm} . Due to the level-pinning enabled by the interplay of dissipative real coupling and coherent imaginary coupling, a fixed frequency $\omega = \omega_0$ in the third-order CT-SR system is always maintained.

mechanism (i.e., imaginary coupling $i\gamma$) and the level repulsion of the coherent coupling mechanism (i.e., real coupling κ) in the system composed of CT and SR. This locked eigenstate can be used to realize the robust WPT.

For the second-order non-Hermitian system composed of the ST and SR, considering the input signal is $s_{1+} = S_{1+}e^{-i\omega t}$, the dynamic equation of the system in Fig. 1(a) can be written as follows [31]:

$$\begin{aligned} \frac{da_1}{dt} &= (-i\omega_0 - g_1 - \Gamma_1) a_1 - i\kappa_0 a_2 + \sqrt{2g_1} s_{1+}, \\ \frac{da_2}{dt} &= (-i\omega_0 - \gamma_2 - \Gamma_2) a_2 - i\kappa_0 a_1, \end{aligned} \quad (1)$$

where g_1 and γ_2 represents the gain and loss between source (load) and transmitter (receiver) coils. Γ_1 and Γ_2 denote intrinsic loss of the harmonic modes $a_n = A_n e^{-i\omega t}$ in transmitter coil and receiver coil, respectively. The power transfer efficiency can be expressed as $\eta = |S_{2-}/S_{1+}|^2$, where output wave corresponds to $S_{2-} = \sqrt{2\gamma_2} A_2$. Considering the zero reflected waves

$S_{1-} = -S_{1+} + \sqrt{2g_1} A_1 = 0$, the power transfer efficiency of the second-order non-Hermitian system can be simplified as [32]

$$\eta = \left| \frac{2\sqrt{g_1\gamma_2}\kappa_0}{\kappa_0^2 + [i(\omega - \omega_0) - (g_1 + \Gamma_1)][i(\omega - \omega_0) - (\gamma_2 + \Gamma_2)]} \right|^2. \quad (2)$$

Consider $\Gamma_1 = \Gamma_2 = \Gamma = 0$, the effective Hamiltonian H can be expressed as [33]

$$H = \begin{pmatrix} \omega_0 + ig_1 & \kappa_0 \\ \kappa_0 & \omega_0 - i\gamma_2 \end{pmatrix}. \quad (3)$$

By solving the characteristic equation $|H - \omega\mathbf{I}| = 0$ (where \mathbf{I} denotes an identity matrix), the eigenvalues of the second-order system can be easily obtained as

$$\omega_{1,2} = \omega_0 + i\frac{g_1 - \gamma_2}{2} \pm \sqrt{\kappa_0^2 - \left(\frac{g_1 + \gamma_2}{2}\right)^2}. \quad (4)$$

For the balanced gain and loss $g_1 = \gamma_2 = \gamma_0$, the system

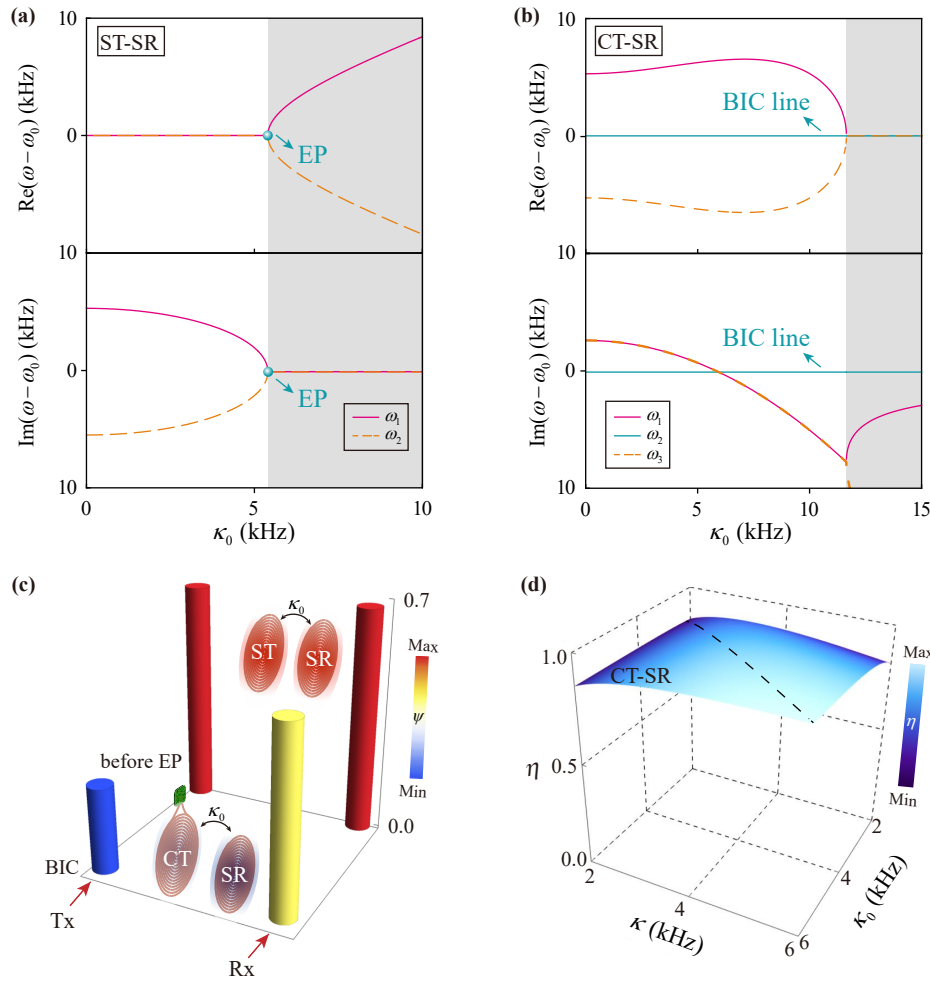


Fig. 2 CT-SR system for high-performance WPT. **(a)** Evolution of the real part and imaginary part of the eigenfrequencies in the PT-symmetric ST-SR system with $g_1 = 5.4$ kHz and $\gamma_2 = 5.4$ kHz. The two splitting eigenvalues collapse at EP. After EP, although the system has a fixed working frequency, the non-zero imaginary part induces a decline of the transfer efficiency. **(b)** Evolution of the real part and imaginary part of the eigenfrequencies in the BIC-assisted CT-SR system with $\kappa = 1.1g_1$, $g_1 = 5.4$ kHz, $\gamma_3 = g_1\kappa_0^2/\kappa^2$. A fixed working frequency $\omega = \omega_0$ corresponding zero imaginary part called BIC is marked by the green line, which can achieve high transfer efficiency. **(c)** Intensity distributions of the ST-SR system ($\omega = \omega_+$) and CT-SR system ($\omega = \omega_0$) for the eigenstate of working frequency in strong coupling region ($g_1 = 5.4$ kHz, $\kappa_0 = 20$ kHz). The inner coupling in CT provided by circuit is 15 kHz. A dark-mode behavior in the CT exists in the BIC-assisted third-order WPT system. **(d)** Transfer efficiency at the fixed working frequency $\omega = \omega_0$ of the BIC-assisted CT-SR system ($g_1 = 5.4$ kHz, $\gamma_3 = g_1\kappa_0^2/\kappa^2$). The intrinsic loss of the resonant coil is $\Gamma = 0.1$ kHz.

satisfies $(PT)H(PT)^{-1} = H$ [34], which is a common approach to realize the real eigenvalues of non-Hermitian systems. The eigenvalues can be described as $\omega_{1,2} = \omega_0 + \sqrt{\kappa_0^2 - \gamma_0^2}$. When $\kappa_0 = \gamma_0$, the two eigenvalues collapse at exceptional point (EP), as shown in Fig. 2(a). However, the realization of real eigenvalues in second-order PT-symmetric system requires operation in the strong coupling region. As the transfer distance increases, the emergence of the imaginary part induces a decline of the transfer efficiency. High-order WPT system is proposed to solve the problem above. For the actual third-order non-Hermitian system composed of CT and SR in Fig. 1(d), the dynamic equation can be represented as [31]

$$\begin{aligned} \frac{da_1}{dt} &= (-i\omega_0 - g_1 - \Gamma_1) a_1 - i\kappa a_2 + \sqrt{2g_1} s_{1+}, \\ \frac{da_2}{dt} &= (-i\omega_0 - \Gamma_2) a_2 - i\kappa a_1 - i\kappa_0 a_3, \\ \frac{da_3}{dt} &= (-i\omega_0 - \gamma_3 - \Gamma_3) a_3 - i\kappa_0 a_2. \end{aligned} \quad (5)$$

Consider $\Gamma_1 = \Gamma_2 = \Gamma_3 = \Gamma = 0$, the effective Hamiltonian of the third-order WPT system with CT coil can be expressed as

$$H = \begin{pmatrix} \omega_0 + ig_1 & \kappa & 0 \\ \kappa & \omega_0 & \kappa_0 \\ 0 & \kappa_0 & \omega_0 - i\gamma_3 \end{pmatrix}, \quad (6)$$

where κ is the inner coupling controlled by circuit, κ_0 is the coupling between CT and SR, g_1 and γ_3 are the actual gain and loss. From the eigenvalue solutions of Eq. (6), we find a new method to realize real eigenvalues. When the equation satisfies $g_1 [(\omega - \omega_0)^2 - \kappa_0^2] = \gamma_3 [(\omega - \omega_0)^2 - \kappa^2]$, the imaginary parts of the eigenfrequencies disappear and the purely real eigenmodes can be obtained [29]. The condition of purely real modes can be summarized into the following two categories:

$$g_1 (\kappa^2 - g_1 \gamma_3) = \gamma_3 (\kappa_0^2 - g_1 \gamma_3),$$

$$\omega_{2,3} = \omega_0 \pm \sqrt{\kappa^2 + \kappa_0^2 - g_1 \gamma_3}, \quad (7)$$

$$g_1 \kappa_0^2 = \gamma_3 \kappa^2, \quad \omega_1 = \omega_0. \quad (8)$$

The real eigenfrequencies in Eq. (7) change with gain or loss and coupling strength, which subsequently gives rise to low stability of WPT system. In contrast, according to Eq. (8), a purely real mode (BIC) independent of gain or loss and coupling strength can be obtained when the criterion is satisfied. The BIC can be realized by adjusting multiple degrees of freedom, which demonstrates that strict PT-symmetry is not a prerequisite for a purely real mode. As shown in Fig. 2(b), the real part and imaginary part of the third-order CT-SR system described by Eq. (6) are plotted. A fixed working frequency always exists where the imaginary part is zero, enabling the maximum transmission efficiency at $\omega = \omega_0$. Corresponding to Eqs. (3) and (6), the intensity distributions of both the conventional ST-SR system and the BIC-assisted CT-SR system for the eigenstate of working frequency are plotted in Fig. 2(c). In strong coupling region (before EP), the working frequency of the ST-SR system is splitting into two modes $\omega = \omega_{\pm}$. The intensity distributions of $\omega = \omega_+$ is plotted by the red cylinder, while the BIC mode $\omega = \omega_0$ of the CT-SR system is plotted by the front blue and yellow cylinder. Since the system is assumed to work in the strong coupling region, we set $g_1 = 5.4$ kHz, $\kappa_0 = 20$ kHz. The inner coupling in CT is 15 kHz. The calculated intensity in ST and SR in the second-order system are both 0.707. However, it can be found that a dark-mode behavior in the CT exists in the BIC-assisted third-order WPT system at the working frequency $\omega = \omega_0$. The intensity in CT and SR are respectively 0.277 and 0.577, which demonstrates that the third-order WPT system based on CT coil can reduce the field leakage from the transmitter coil, thus ensuring better electromagnetic compatibility.

Combining the output wave $S_{2-} = \sqrt{2\gamma_3}A_3$ and Eq. (5), the transfer efficiency of the third-order CT-SR system with actual intrinsic loss $\Gamma_1 = \Gamma_2 = \Gamma_3 = \Gamma \neq 0$ at $\omega = \omega_0$ can be described as

$$\eta = |S_{21}|^2 = \left| -\frac{2\sqrt{g_1\gamma_3\kappa\kappa_0}}{g_1\kappa_0^2 + \gamma_3\kappa^2 + (\kappa^2 + \kappa_0^2 + g_1\gamma_3)\Gamma + (g_1 + \gamma_3)\Gamma^2 + \Gamma^3} \right|^2. \quad (9)$$

In special cases, when $g_1 = \gamma_3$ and $\kappa = \kappa_0$, the system satisfies PT-symmetry [35]. The transfer efficiency of the BIC-assisted CT-SR system ($g_1 = 5.4$ kHz, $\gamma_3 = g_1\kappa_0^2/\kappa^2$) is calculated in Fig. 2(d). With the aid of BIC, the system can achieve efficient WPT for arbitrary values of coupling strength, provided they satisfy $\gamma_3 = g_1\kappa_0^2/\kappa^2$. To be noted, due to the non-negligible intrinsic losses $\Gamma = 0.1$ kHz, the maximum efficiency of WPT system is limited to 90%.

Figures 3(a)–(f) display the eigenfrequency (both real and imaginary components) of the third-order CT-SR system as functions of transfer distance under varying gain-loss ratios, i.e., $\gamma_3 = 2g_1$, $\gamma_3 = g_1$, $\gamma_3 = 0.5g_1$, respectively. BICs plotted by green points have zero imaginary part and fixed real part $\omega = \omega_0$. Assuming that $\kappa = 1.5g_1$, $g_1 = 5.4$ kHz, BIC occurs at specific transfer distances, which satisfy $\gamma_3 = g_1\kappa_0^2/\kappa^2$, corresponding to the maximum efficiency as shown by the blue lines in Figs. 3(d)–(f). The results in Fig. 3 indicate that BIC can be achieved through flexible tuning of gain, loss and coupling strength, without requiring strict PT-symmetry. Here, we fixed g_1 and κ while adjusting the γ_3 (load) and κ_0 , but actually the system allows arbitrary parameter tuning provided they satisfy the equation $\gamma_3 = g_1\kappa_0^2/\kappa^2$.

3 Experiment

Practical WPT applications require not only stability but also high efficiency and integrated miniaturization, which remain challenges that currently limit widespread implementation. Inspired by novel synthetic-dimensional physics [36–38], here we construct the BIC-assisted third-order non-Hermitian WPT system based on an artificial CT coil. The schematic diagram of the synthetic WPT system is shown in Fig. 4(a). The experimental lumped electronic components for the synthetic CT are outlined in yellow dashes. Details can be seen in the enlarged inset. L_2 and L_3 are the distributed inductances constructed by the Litz wire, while L_1 and C_i ($i = 0, 1, 2$) are lumped inductance and capacitor, respectively. The corresponding effective circuit model of the synthetic third-order WPT system is shown in Fig. 1(e). Considering $L_1 = L_2 = L_3 = L$, $C_1 = C_2$ and $C = C_0C_1/(C_0 + C_1)$, we can get the dynamic equation of the synthetic BIC-assisted third-order non-Hermitian WPT system as [30] (more details about the dynamic equation derived from Kirchhoff's equations are introduced in the Supplementary Note 2):

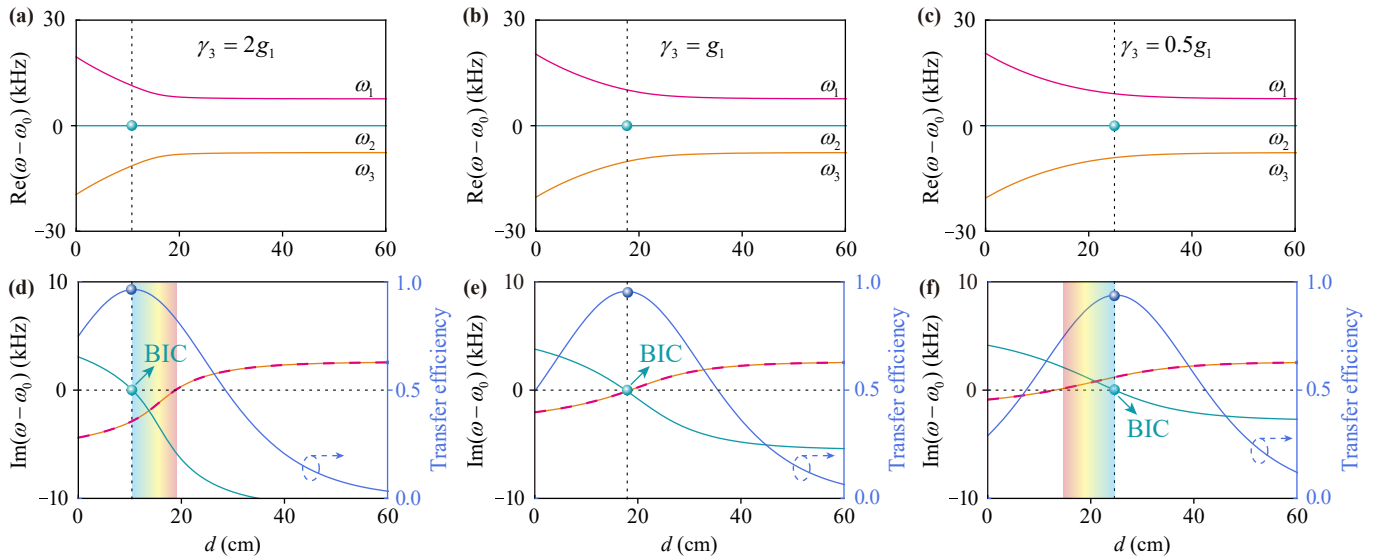


Fig. 3 Flexible manipulation of the BIC for efficient WPT in the third-order CT-SR system. Evolution of the (a–c) real part and (d–f) imaginary part of the eigenfrequencies with different gain-loss ratios $\gamma_3 = 2g_1$, $\gamma_3 = g_1$, $\gamma_3 = 0.5g_1$, respectively. The parameter set is $\kappa = 1.5g_1$, $g_1 = 5.4$ kHz. BIC plotted by green and blue points occurs at specific transfer distances, which satisfy $\gamma_3 = g_1\kappa_0^2/\kappa^2$. The blue line is the transfer efficiency as a function of transfer distance. The position of BIC corresponding to zero imaginary part reaches the maximum efficiency. The intrinsic loss is $\Gamma = 0.1$ kHz.

$$\begin{pmatrix} \omega - \omega_0 + i\frac{Z}{2L} & -\frac{1}{2\omega_0 C_0 L} & 0 \\ -\frac{1}{2\omega_0 C_0 L} & \omega - \omega_0 & \frac{M\omega_0}{2L} \\ 0 & \frac{M\omega_0}{2L} & \omega - \omega_0 - i\frac{R}{2L} \end{pmatrix} \begin{pmatrix} a_1 \\ a_2 \\ a_3 \end{pmatrix} = 0, \quad (10)$$

where M is mutual inductance between the CT coil and receiver coil constructed by the distributed inductance L_2 and L_3 . Corresponding to Eq. (6), $g_1 = Z/(2L)$, $\gamma_3 = R/(2L)$ and $\kappa = 1/(2\omega_0 C_0 L)$. When the system works at the fixed frequency $\omega = \omega_0$, κ can be reformulated as $\kappa = \omega_0 C/(2C_0)$. In actual system, we set $L = 737$ μH , $C_0 = 44$ nF, $C_1 = 5.1$ nF, $C = 4.57$ nF and $Z = 50$ Ω . γ_3 can be flexibly tuned by changing the load R to match κ_0 with the increase of transfer distance. In the experiment, the load R changes from 3.5 Ω to 30 Ω . Signal is input from the ‘+’ and ‘−’ on the left of the circuit board, as shown in the inset of Fig. 4(a). The radius of the synthetic CT is 30 cm. Under the near-field coupling mechanism, the coupling strength between the CT coil and the receiver coil decreases exponentially with the distance increase as $\kappa_0 = 19.1457e^{-0.048d}$ kHz (details are provided in the Supplementary Note 3). The eigenfrequency $f_0 = \omega_0/(2\pi)$ is 86.5 kHz, which remains independent of gain, loss and coupling, as shown in Fig. 2(b).

Here, we use an actual power signal source (AG 1006, source impedance 50 Ω) to demonstrate the high efficiency of the BIC-assisted third-order WPT system based on CT coil. The SR is equipped with an LED lamp (3W) to directly show the high efficiency of BIC-assisted third-

order WPT system. In both the PT-symmetric ST-SR system and BIC-assisted CT-SR system, the input of power signal source is 5 W at the working frequency, with the distance $d = 51$ cm. Comparing the two pictures in Fig. 4(b), the LED in the CT-SR system can be lit up, but the LED in the ST-SR system remains dark. Transfer efficiency at more transfer distance is plotted in Fig. 4(c). According to Eqs. (2) and (9), the calculated transfer efficiency of the conventional ST-SR system and the optimized CT-SR system is given by the purple dashed line and green solid line under the same transfer distance. The actual transfer efficiency is measured by a differential voltage probe (DVP, ETA5010), which is presented by purple and green symbols(details are provided in the Supplementary Note 4). It can be clearly seen that the BIC-assisted third-order WPT system based on CT coil has superior efficiency to the second-order PT-symmetric WPT system when the system works at a fixed working frequency $\omega = \omega_0$ at the same transfer distance. To be noted that, the efficiency of the third-order system is slightly lower than that of the second-order system in strong coupling region because the intrinsic loss of the third-order system is a little higher. The BIC-assisted third-order WPT system relaxes strict symmetry requirements and enables flexible parameter tuning. Then, we evaluate the idle power loss in the idle state without SR for two types of WPT schemes in Fig. 4(d). Consider $C_0 = 22$ nF, $C_1 = 5.8$ nF, $C = 4.59$ nF, the calculated and measured idle power loss of the conventional (optimized) WPT system with ST-SR (CT-SR) is marked by the dashed purple (solid green) line and purple (green) symbols, respectively. The

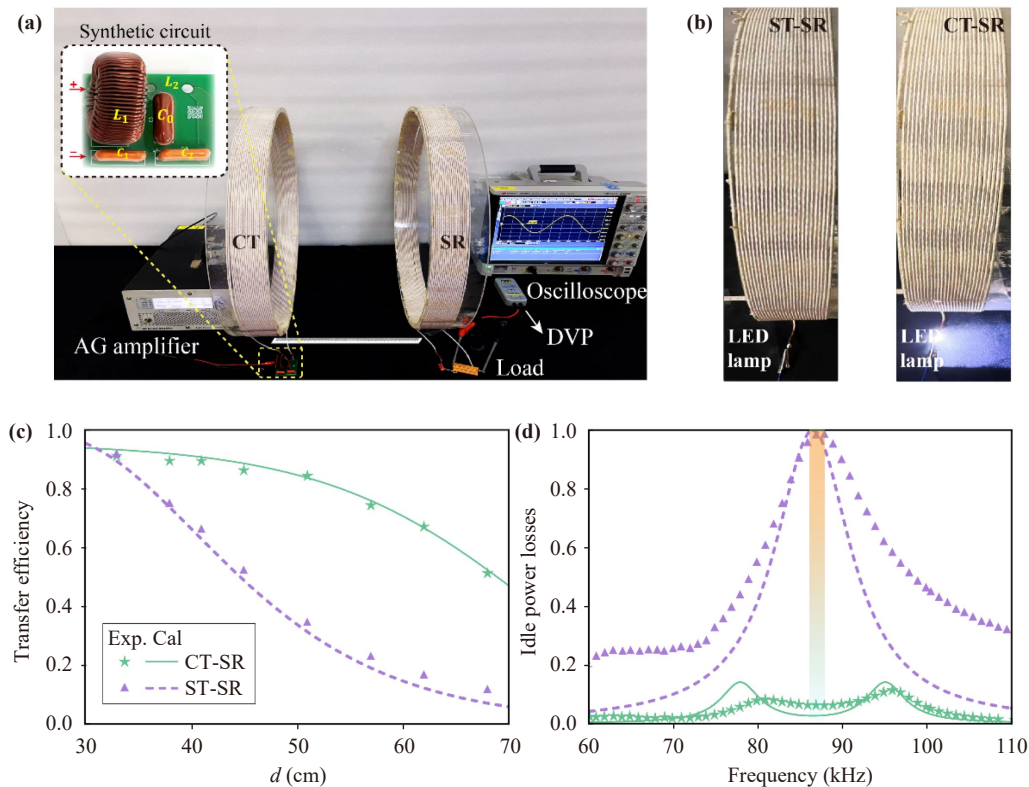


Fig. 4 Experiment comparison of PT-symmetric ST-SR system and BIC-assisted CT-SR system. **(a)** Experimental setup of the CT-SR system. Detailed information of the lumped electronic components for the synthetic CT coil provided in the inset. The signal is input from the ‘+’ and ‘-’ on the left. L_2 is the distributed inductance provided by the coil. The load R changes from 3.5Ω to 30Ω to match the increase of transfer distance. The actual transfer efficiency is measured by a DVP connected to the oscilloscope. **(b)** Experimental demonstration of the ST-SR system and CT-SR system by lighting two LED lamps on SR. The LED in the CT-SR system can be lit up, while the LED in the ST-SR system remains dark at the same transfer distance. **(c)** Measured(calculated) transfer efficiency of the CT-SR system and ST-SR system when they work at a fixed working frequency $\omega = \omega_0$ at the same transfer distance. With the aid of BIC, the CT-SR system has superior efficiency. **(d)** Measured(calculated) idle power loss plotted by symbols (lines). The optimized CT-SR system exhibits significantly lower idle power loss near the operating frequency compared to the conventional ST-SR system.

optimized WPT system exhibits significantly lower idle power loss near the operating frequency compared to the conventional theoretical case, which is conducive to intermittent wireless charging and energy saving in practical applications.

4 Conclusion

In summary, the efficient BIC-assisted third-order WPT system based on CT coil is theoretically proposed and experimentally realized in this work. Compared with the conventional second-order PT-symmetric system based on ST coil, the CT-SR system always has a fixed purely real working frequency and can achieve high efficiency even in weak coupling region. Notably, strict PT-symmetry is not necessary for BIC realization, which relaxes symmetry constraints and facilitates parameter tuning in practical applications. Moreover, the CT structure can realize highly integrated systems and enable

better electromagnetic compatibility in the transmitter. In addition, the proposed WPT mechanism may be extended in anti-PT symmetric systems [39, 40]. The CT structure can also be used to construct coupled chains, allowing for the incorporation of topological physics to achieve robust and efficient WPT [41, 42]. The results for BIC-assisted third-order WPT system based on CT coil not only achieve high performance WPT (higher transfer efficiency, better electromagnetic compatibility, and lower standby power loss) than conventional second-order PT-symmetric system, but also provides a good platform to realize miniaturized and integrated high-order non-Hermitian WPT systems.

Declarations The authors declare that they have no competing interests and there are no conflicts.

Data and code availability All the data that support the findings of this study are available from the corresponding authors upon reasonable request.

Code availability All the codes that support the findings of this study are available from the corresponding authors upon reasonable request.

Electronic supplementary materials The online version contains supplementary material available at <https://doi.org/10.15302/frontphys.2026.045202>.

Acknowledgements This work was supported by the National Key R&D Program of China (Nos. 2023YFA1407600 and 2021YFA1400602), the National Natural Science Foundation of China (Nos. 12374294 and 52477014), and the Chenguang Program of Shanghai Education Development Foundation and Shanghai Municipal Education Commission (No. 21CGA22).

References

1. Q. Li and Y. C. Liang, An inductive power transfer system with a high- Q resonant tank for mobile device charging, *IEEE Trans. Power Electron.* 30, 6203 (2015)
2. C. C. Mi, G. Buja, S. Y. Choi, and C. T. Rim, Modern advances in wireless power transfer systems for roadway powered electric vehicles, *IEEE Trans. Ind. Electron.* 63, 6533 (2016)
3. K. Sun, R. Fan, X. Zhang, Z. Zhang, Z. Shi, N. Wang, P. Xie, Z. Wang, G. Fan, H. Liu, C. Liu, T. Li, C. Yan, and Z. Guo, An overview of metamaterials and their achievements in wireless power transfer, *J. Mater. Chem. C* 6(12), 2925 (2018)
4. Y. Chen, W. Xiao, Z. Guan, B. Zhang, D. Qiu, and M. Wu, Nonlinear modeling and harmonic analysis of magnetic resonant WPT system based on equivalent small parameter method, *IEEE Trans. Ind. Electron.* 66, 6604 (2019)
5. A. Kurs, A. Karalis, R. Moffatt, J. D. Joannopoulos, P. Fisher, and M. Soljačić, Wireless power transfer via strongly coupled magnetic resonances, *Science* 317(5834), 83 (2007)
6. A. P. Sample, D. T. Meyer, and J. R. Smith, Analysis, experimental results, and range adaptation of magnetically coupled resonators for wireless power transfer, *IEEE Trans. Ind. Electron.* 58(2), 544 (2011)
7. Y. Wu, L. Kang, D. H. Werner, and P. T. Generalized, Symmetry in non-Hermitian wireless power transfer systems, *Phys. Rev. Lett.* 129(20), 200201 (2022)
8. C. Liang, Y. Tang, A. Xu, and Y. Liu, Observation of exceptional points in thermal atomic ensembles, *Phys. Rev. Lett.* 130(26), 263601 (2023)
9. R. El-Ganainy, K. G. Makris, M. Khajavikhan, Z. H. Musslimani, S. Rotter, and D. N. Christodoulides, Non-Hermitian physics and PT symmetry, *Nat. Phys.* 14(1), 11 (2018)
10. C. M. Bender and S. Boettcher, Real spectra in Non-Hermitian Hamiltonians having PT symmetry, *Phys. Rev. Lett.* 80(24), 5243 (1998)
11. J. Schindler, Z. Lin, J. M. Lee, H. Ramezani, F. M. Ellis, and T. Kottos, PT-symmetric electronics, *J. Phys. A* 45(44), 444029 (2012)
12. Z. Guo, J. Jiang, Y. Wang, J. Alvarez-Cuervo, A. T. Martin-Luengo, S. Hu, J. Jiang, P. A. Gonzalez, J. Duan, and H. Chen, Exceptional point empowered near-field routing of hyperbolic polaritons, *Sci. Bull. (Beijing)* 69(22), 3491 (2024)
13. Z. Chen, X. Sun, W. Song, P. Wheeler, J. Liu, and B. Ren, Maximum efficiency tracking control for omnidirectional wireless power transfer system based on AdamW algorithm, *IEEE Trans. Power Electron.* 40(3), 4602 (2025)
14. H. Li, J. Li, K. Wang, W. Chen, and X. Yang, A maximum efficiency point tracking control scheme for wireless power transfer systems using magnetic resonant coupling, *IEEE Trans. Power Electron.* 30(7), 3998 (2015)
15. J. Zhou, B. Zhang, W. Xiao, D. Qiu, and Y. Chen, Nonlinear parity-time-symmetric model for constant efficiency wireless power transfer: Application to a drone-in-flight wireless charging platform, *IEEE Trans. Ind. Electron.* 66(5), 4097 (2019)
16. A. U. Hassan, H. Hodaie, M. A. Miri, M. Khajavikhan, and D. N. Christodoulides, Nonlinear reversal of the PT-symmetric phase transition in a system of coupled semiconductor microring resonators, *Phys. Rev. A* 92(6), 063807 (2015)
17. S. Assaworrorarit, X. Yu, and S. Fan, Robust wireless power transfer using a nonlinear parity-time-symmetric circuit, *Nature* 546(7658), 387 (2017)
18. Z. Wei and B. Zhang, Transmission range extension of PT-symmetry-based wireless power transfer system, *IEEE Trans. Power Electron.* 36(10), 11135 (2021)
19. X. Hao, K. Yin, J. Zou, R. Wang, Y. Huang, X. Ma, and T. Dong, Frequency-stable robust wireless power transfer based on high-order pseudo-Hermitian physics, *Phys. Rev. Lett.* 130(7), 077202 (2023)
20. Y. R. Zhang, Z. Z. Zhang, J. Q. Yuan, M. Kang, and J. Chen, High-order exceptional points in non-Hermitian Moiré lattices, *Front. Phys. (Beijing)* 14(5), 53603 (2019)
21. F. Mohseni, A. Hakimi, A. Nikzamir, H. Cao, and F. Capolino, One-transmitter-multiple-receiver system for wireless power transfer using an exceptional point of degeneracy, *Phys. Rev. Appl.* 23(5), 054046 (2025)
22. Z. Guo, J. Jiang, X. Wu, H. Zhang, S. Hu, Y. Wang, Y. Li, Y. Yang, H. Chen, Rotation manipulation of high-order PT-symmetry for robust wireless power transfer, *Fundamental Res.*, doi: 10.1016/j.fmre.2023.11.010 (2023)
23. S. Zhao, Y. Fan, R. Yang, Z. Ye, F. Zhang, C. Wang, W. Luo, Y. Wen, and J. Zhou, Smart reconfigurable metadivices made of shape memory alloy metamaterials, *Opto-Electron. Adv.* 8(2), 240109 (2025)
24. C. W. Hsu, B. Zhen, A. D. Stone, J. D. Joannopoulos, and M. Soljačić, Bound states in the continuum, *Nat. Rev. Mater.* 1(9), 16048 (2016)
25. N. Cortés, L. Chico, M. Pacheco, L. Rosales, and P. A. Orellana, Bound states in the continuum: Localization of Dirac-like fermions, *Europhys. Lett.* 108(4), 46008 (2014)
26. Y. Plotnik, O. Peleg, F. Dreisow, M. Heinrich, S. Nolte, A. Szameit, and M. Segev, Experimental observation of optical bound states in the continuum, *Phys. Rev. Lett.* 107, 183901 (2011)



27. Q. Wang, C. Zhu, X. Zheng, H. Xue, B. Zhang, and Y. D. Chong, Continuum of bound states in a non-Hermitian model, *Phys. Rev. Lett.* 130, 103602 (2023)
28. Y. Liang, K. Koshelev, F. Zhang, H. Lin, S. Lin, J. Wu, B. Jia, and Y. Kivshar, Bound states in the continuum in anisotropic plasmonic metasurfaces, *Nano Lett.* 20(9), 6351 (2020)
29. H. Zhang, Z. Guo, Y. Li, Y. Yang, Y. Chen, and H. Chen, A universal non-Hermitian platform for bound state in the continuum enhanced wireless power transfer, *Front. Phys. (Beijing)* 19(4), 43209 (2024)
30. Z. Guo, F. Yang, H. Zhang, X. Wu, Q. Wu, K. Zhu, J. Jiang, H. Jiang, Y. Yang, Y. Li, and H. Chen, Level pinning of anti-PT-symmetric circuits for efficient wireless power transfer, *Natl. Sci. Rev.* 11(1), nwad172 (2023)
31. C. Zeng, Z. Guo, K. Zhu, C. Fan, G. Li, J. Jiang, Y. Li, H. Jiang, Y. Yang, Y. Sun, and H. Chen, Efficient and stable wireless power transfer based on the non-Hermitian physics, *Chin. Phys. B* 31(1), 010307 (2022)
32. S. Fan, W. Suh, and J. D. Joannopoulos, Temporal coupled-mode theory for the Fano resonance in optical resonators, *J. Opt. Soc. Am. A* 20(3), 569 (2003)
33. L. Wang, Y. Wang, Z. Guo, H. Jiang, Y. Li, Y. Yang, and H. Chen, Research progress of magnetic resonance wireless power transfer based on higher-order non-Hermitian physics, *Acta Phys. Sin.* 73(20), 201101 (2024)
34. S. Weimann, M. Kremer, Y. Plotnik, Y. Lumer, S. Nolte, K. G. Makris, M. Segev, M. C. Rechtsman, and A. Szameit, Topologically protected bound states in photonic parity-time-symmetric crystals, *Nat. Mater.* 16(4), 433 (2017)
35. P. Chen, M. Sakhdari, M. Hajizadegan, Q. Cui, M. M. C. Cheng, R. El-Ganainy, and A. Alù, Generalized parity-time symmetry condition for enhanced sensor telemetry, *Nat. Electron.* 1(5), 297 (2018)
36. Z. Guo, Y. Long, H. Jiang, J. Ren, and H. Chen, Anomalous unidirectional excitation of high- k hyperbolic modes using all-electric metasources, *Adv. Photonics* 3(3), 036001 (2021)
37. L. Yuan, Q. Lin, M. Xiao, and S. Fan, Synthetic dimension in photonics, *Optica* 5(11), 1396 (2018)
38. L. Yuan, D. Wang, and S. Fan, Synthetic gauge potential and effective magnetic field in a Raman medium undergoing molecular modulation, *Phys. Rev. A* 95(3), 033801 (2017)
39. C. Li, R. Yang, X. Huang, Q. Fu, Y. Fan, and F. Zhang, Experimental demonstration of controllable PT and anti-PT coupling in a non-Hermitian metamaterial, *Phys. Rev. Lett.* 132(15), 156601 (2024)
40. L. Wang, S. Hu, Y. Sun, H. Jiang, Y. Li, Y. Yang, H. Chen, and Z. Guo, Higher-order anti-PT symmetry for efficient wireless power transfer in multiple-transmitter system, *Front. Phys. (Beijing)* 20(5), 54201 (2025)
41. R. Lin, T. Tai, L. Li, and C. H. Lee, Topological non-Hermitian skin effect, *Front. Phys. (Beijing)* 18(5), 53605 (2023)
42. L. Wan, Y. Li, Y. Yang, H. Chen, and Z. Guo, Large-area topological wireless power transfer, *Front. Phys. (Beijing)* 21(1), 14200 (2026)